Microporous and Mesoporous Materials 382 (2025) 113391

Contents lists available at ScienceDirect

Microporous and Mesoporous Materials

journal homepage: www.elsevier.com/locate/micromeso

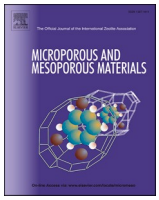

Preparation and characterization of Santa Barbara Amorphous-15 particles functionalized with mercaptopropyl groups and of their composites with poly(lactic acid)

Tamara M. Díez-Rodríguez [a,**], Enrique Blázquez-Blázquez [a], João P. Lourenço [b,c], Juan C. Martínez [d], María L. Cerrada [a,*], Ernesto Pérez [a]

[a] Instituto de Ciencia y Tecnología de Polímeros (ICTP-CSIC), Juan de la Cierva 3, 28006, Madrid, Spain
[b] Faculdade de Ciências e Tecnologia, Universidade do Algarve, Campus de Gambelas, 8005-139, Faro, Portugal
[c] Centro de Química Estrutural, Institute of Molecular Sciences, Instituto Superior Técnico, Universidade de Lisboa, Av. Rovisco Pais, 1049-001, Lisboa, Portugal
[d] CELLS, ALBA Synchrotron Light Source, Carrer de la Llum 2-26, 08290, Cerdanyola del Vallès, Barcelona, Spain

ARTICLE INFO

Keywords:
PLA
Functionalized SBA-15
Mercaptopropyl groups
Nucleation capacity
Cold crystallization
Crystal structure

ABSTRACT

Santa Barbara Amorphous-15 (SBA-15) particles functionalized with mercaptopropyl groups (named as SBASH) have been prepared by a synthetic one-pot approach, and then have been incorporated into poly(lactic acid) (PLA), comparing their characteristics with those shown by composites attained with neat SBA-15 (PLASBA). The silica including the mercaptopropyl groups exhibits a certain loss of regularity because of its functionalization, although displays a better interaction with PLA than the pristine SBA-15 particles in the resulting materials. These composites (PLASBASH and PLASBA) also show a thermal stability slightly higher than neat PLA. An important nucleation effect of SBASH silica in the crystallization of PLA has been deduced from cooling experiments as well as from the cold crystallization in heating runs and from the degree of crystallinity reached. Small Angle X-ray Scattering (SAXS) profiles show that the PLA long spacings are rather similar for the different composites and the neat PLA. Thus, crystal size is rather similar in all samples. Microhardness values show an evident effect of reinforcement in all the composites compared with that shown by neat PLA. Nevertheless, the increase in rigidity is smaller in the biobased PLASBASH composites, those containing the modified silica, than in the PLASBA materials with the pristine SBA-15 particles.

1. Introduction

Polylactic acid (PLA) is a linear aliphatic thermoplastic, produced from natural polysaccharides such as corn, sugar cane or cassava. It is prepared through the grafting polymerization of lactic acid or ring-opening polymerization of lactide [1–4]. Thus, PLA stands out as one of the most promising biodegradable alternatives to traditional petroleum-based plastics for industrial applications [5].

Nevertheless, pristine PLA shows certain limitations in terms of its properties, processing and use. The former includes low crystallization rate, brittleness, poor toughness, and low temperature resistance [2,6]. Consequently, improving the overall performance of PLA has become a priority in research. Melt-blending with ductile polymers and the addition of inorganic additives are expected to overcome some of the above PLA drawbacks. The effect of montmorillonite and talc has been widely investigated [6–10].

Dispersion and interfacial adhesion of those minor components within PLA matrices are key aspects in the development of high-performance PLA-based composites. Thus, surface modification with silanes is one of the most used approaches to achieve this desired compatibility between the different phases [11–16]. Incorporation of plasticizers is another very interesting method to improve the interfacial interactions between PLA and different fillers [17–20].

Concerning mesoporous silica particles, it should be said that they display some singular characteristics, including their very large internal surface areas and pore volumes together with a high thermal stability and capability for an easy superficial modification, among others. The most commonly used mesoporous silicas are Mobil Composition of

* Corresponding author.
** Corresponding author.
E-mail addresses: t.diez@ictp.csic.es (T.M. Díez-Rodríguez), mlcerrada@ictp.csic.es (M.L. Cerrada).

https://doi.org/10.1016/j.micromeso.2024.113391
Received 17 June 2024; Received in revised form 7 October 2024; Accepted 22 October 2024
Available online 23 October 2024
1387-1811/

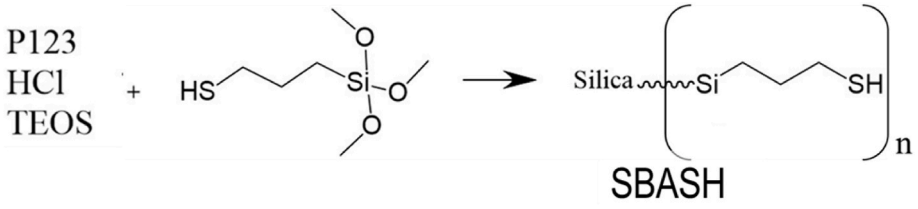

Scheme 1. Detail of the one-pot synthesis of SBASH particles: SBA-15 functionalized with the mercaptopropyl group.

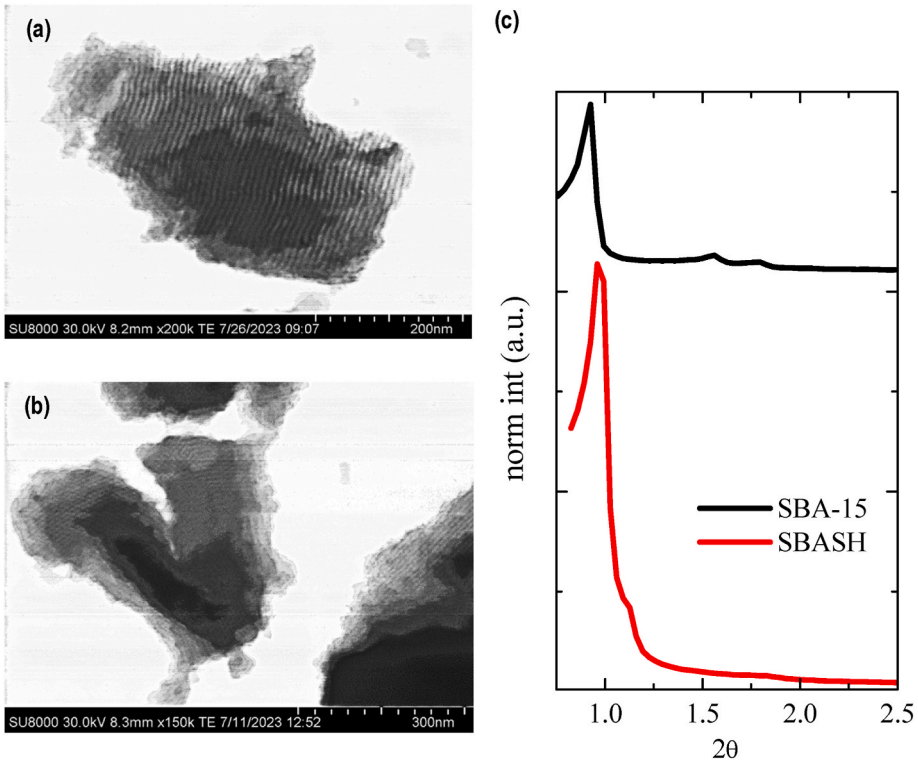

Fig. 1. FESEM images for (a) SBA-15 and (b) SBASH particles: scale bar of 200 nm (top) and of 300 nm (bottom). (c) WAXD profiles of SBA-15 and SBASH silicas.

Matter No. 41 (MCM-41) [21] and SBA-15 [22], both of them with regular pores disposed in a hexagonal arrangement. They were firstly synthesized at the end of the 20th century [23,24], and different investigations have attempted since then to develop new silicas with additional and innovative features. Thus, hybrid mesoporous silicas loaded with different compounds have been described in literature following post-functionalization approaches by chemical modification with metals [25,26], ceramics [27–29] or even polymers [30–34].

These modified mesoporous silicas can be also achieved by one-pot synthetic methods. These procedures require incorporation of the new compound during the stage of synthesis. Changes in the internal structure and important damages of the porous characteristics, leading even to the complete disappearance of the internal order, can take place, however, through this methodology. Therefore, the control of silica coating thickness [35,36] and ways to increase pore size [27,37] have been investigated.

Mesoporous silicas, pristine or functionalized, can be also used as polymer modifiers leading to the subsequent composites. In such case, confinement phenomena of the polymeric chains within the empty pores of the mesoporous particles [38,39] can take place. Furthermore, the contact between the polymer and the silica is expected not to be very intimate because of their different chemical nature, rather hydrophobic for most of polymers versus very hydrophilic for silica. A feasible way for improving the interactions between both components, polymer and silica, is to functionalize the silica incorporating organic groups into it, taking advantage of its facility for being modified.

Thus, the main objective of this research is to evaluate the effect of decorating SBA-15 particles with mercaptopropyl groups, using a one-pot approach, on the global behavior of PLA based composites in which this mesoporous hybrid silica is incorporated, and to further compare their performances with those exhibited by PLA materials containing pristine SBA-15 particles. For that, composites of PLA are prepared at different contents using neat and modified mesoporous silicas, synthesized both in the laboratory. Additionally to the synthesis of both silicas (pristine and functionalized) and the further obtainment of composites from their incorporation into the PLA matrix, different techniques have been used for their characterization, namely Scanning Electron Microscopy (SEM), Thermogravimetric Analysis (TGA), Differential Scanning Calorimetry (DSC) and X-ray Diffraction, using both conventional and real-time variable-temperature synchrotron radiation. Moreover microhardness (MH) measurements have been also performed to study preliminarily the mechanical properties of these composites.

2. Experimental part

2.1. Materials and chemicals

A commercially available *L*-rich polylactide (PLA) from

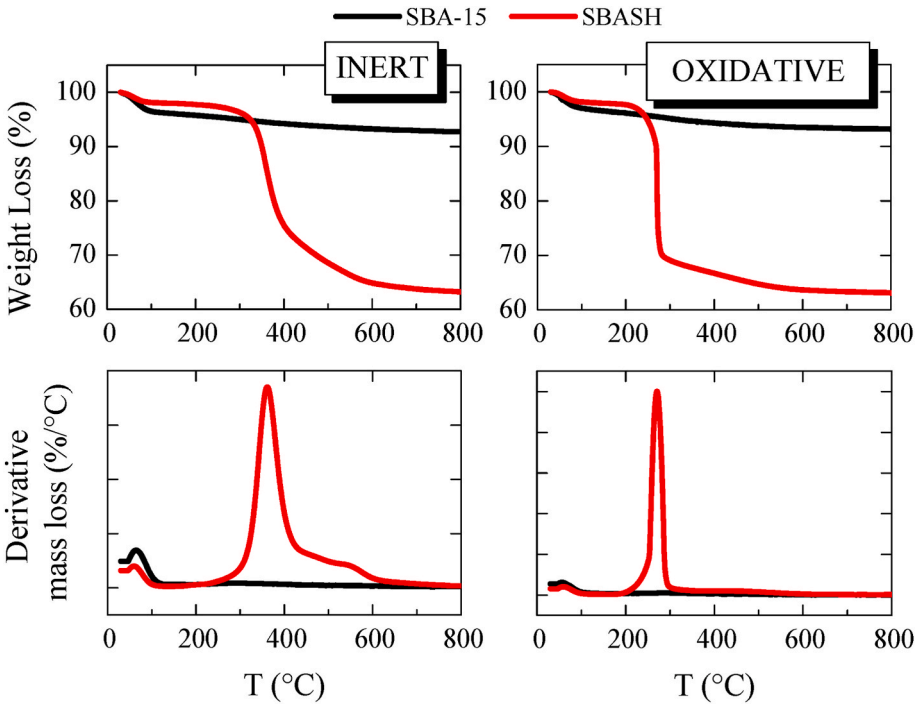

Fig. 2. TGA curves (top representations) and their corresponding derivatives (bottom plots) under inert (left) and oxidative (right) atmospheres for the SBA-15 and SBASH particles.

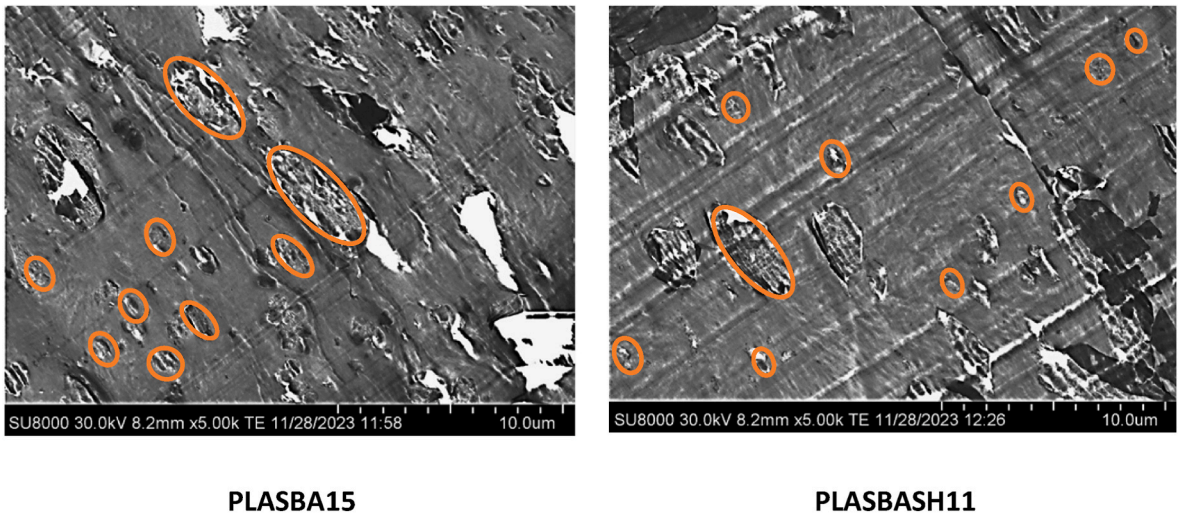

Fig. 3. FESEM micrographs for PLASBA15 (left) and PLASBASH11 (right) composites, with relevant features marked.

NatureWorks® (labeled as Ingeo™ Biopolymer 6202D, with a density of 1.24 g/cm^3, and a content in *L*-isomer units of about 98 mol%) is used in this study. Its weight-average molecular weight, M_w, is 118,600 g/mol, with a molecular weight dispersity of 1.6, as determined from gel permeation chromatography (GPC) [40].

Poly(ethylene glycol) *block*–poly(propylene glycol) *block*–poly (ethylene glycol) (P123), tetraethyl orthosilicate (TEOS), 3-mercapto-propyltrimetoxysilane, and HCl (37 %), purchased from Sigma-Aldrich, and NaCl from MERCK have been used for synthesizing the mesoporous silicas.

2.2. Synthesis of SBA-15 and SBASH particles

SBA-15 was synthetized following the protocol previously described in the literature [41]. In brief, 10.7 g of P123 and 405 g of H_2O were stirred at room temperature until solution. Then, 37 mL of HCl and 25 g of TEOS were added, followed by the addition (after *ca.* 2h) of 10 g of NaCl. The final mixture was left stirring overnight at 40 °C. The solution was kept 3 days at 100 °C in an oven, then was centrifuged and washed to eliminate the acid. The template was partially removed by extraction with ethanol 96 % at reflux temperature overnight. The product was recovered, dried, and finally treated at 550 °C for 7h under a flow of dry air.

Synthesis of the hybrid SBA-15 particles with mercaptopropyl groups (SBASH), using a one-pot protocol, follows the same procedure just described, employing different amounts of the reagents (20 g P123, 490 g H_2O, 8.2 mL HCl, 38.9 g TEOS) and incorporating 4.1 g of 3-mercaptopropyltrimetoxysilane before the addition of TEOS. In this case, the extraction procedure was repeated, and no high temperature treatment was carried out. A sketch of this reaction is shown in Scheme 1.

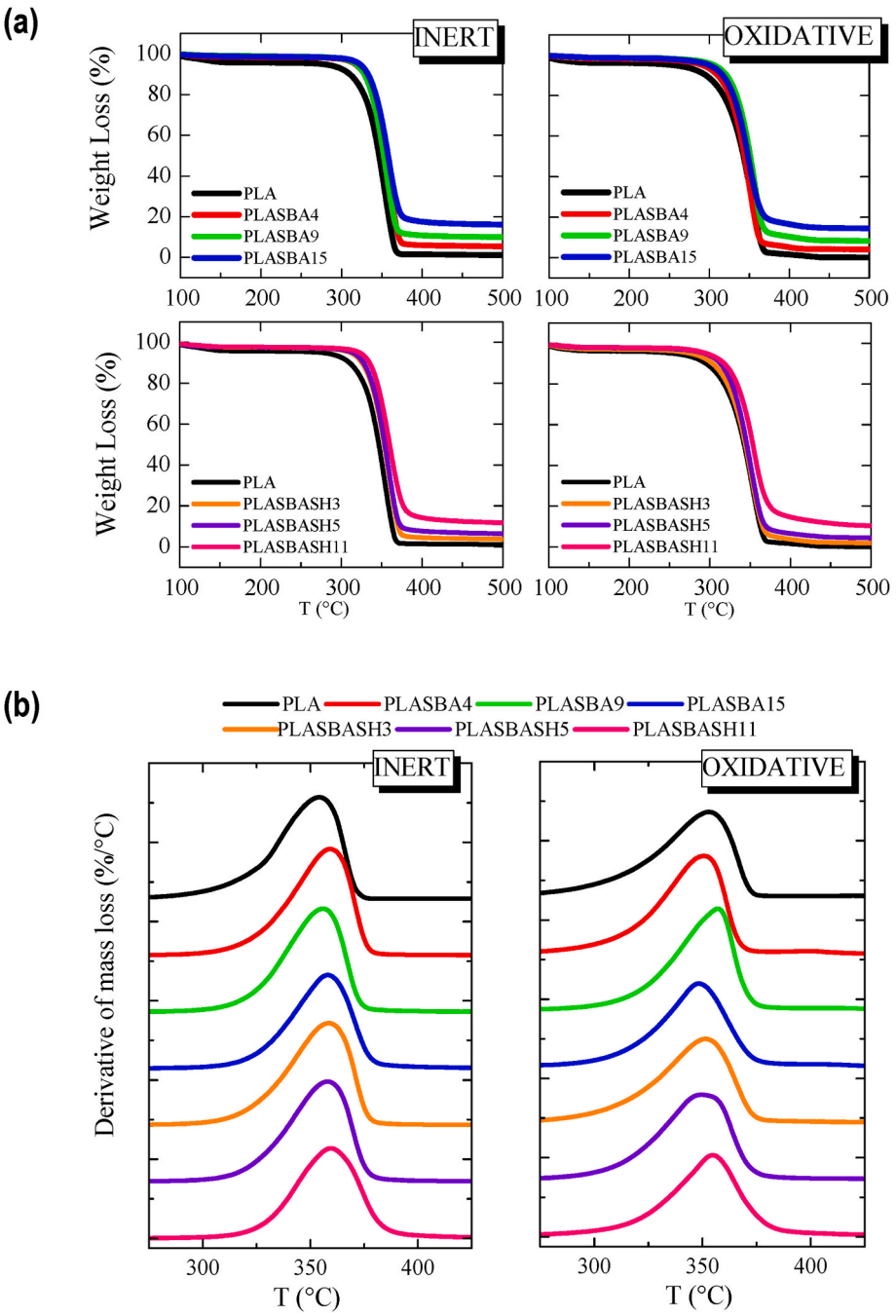

Fig. 4. TGA (a) and DTGA (b) curves for PLA composites with SBA-15 or SBASH under nitrogen (left plots) and under air (right representations), respectively.

Table 1
Average silica content (determined from the 2 atm), and temperature at the maximum in the DTGA curves (T_{max}^{DTGA}) under air and nitrogen environments for the PLA composites with SBA-15 or SBASH silicas.

Sample	Silica content (wt.%)	T_{max}^{DTGA} (°C)	
		Air	Nitrogen
PLA	0	352.7	354.1
PLASBA4	4.4	350.6	359.1
PLASBA9	8.7	357.0	355.9
PLASBA15	14.9	348.3	358.0
PLASBASH3	2.9	358.6	351.4
PLASBASH5	5.4	358.0	349.4
PLASBASH11	11.1	359.5	354.7

2.3. Preparation of composites

Composites with different contents in either pristine SBA-15 or hybrid SBASH particles were achieved as follows [42]: an appropriate amount of pure SBA-15 or SBASH silica was dispersed in chloroform at the same time that a PLA/chloroform solution (6 wt% in PLA) was prepared. Both, dispersion and solution, were stirred for 18 h at room temperature. Afterwards, the dispersion containing neat or hybrid SBA-15 particles was added to the PLA/chloroform solution and this PLA/silica/chloroform dispersion was additionally stirred for 6 h at room temperature before it was poured into Petri dishes and dried at room temperature for 48 h. The resultant composite films were additionally dried under vacuum in an oven at 85 °C for 2 h.

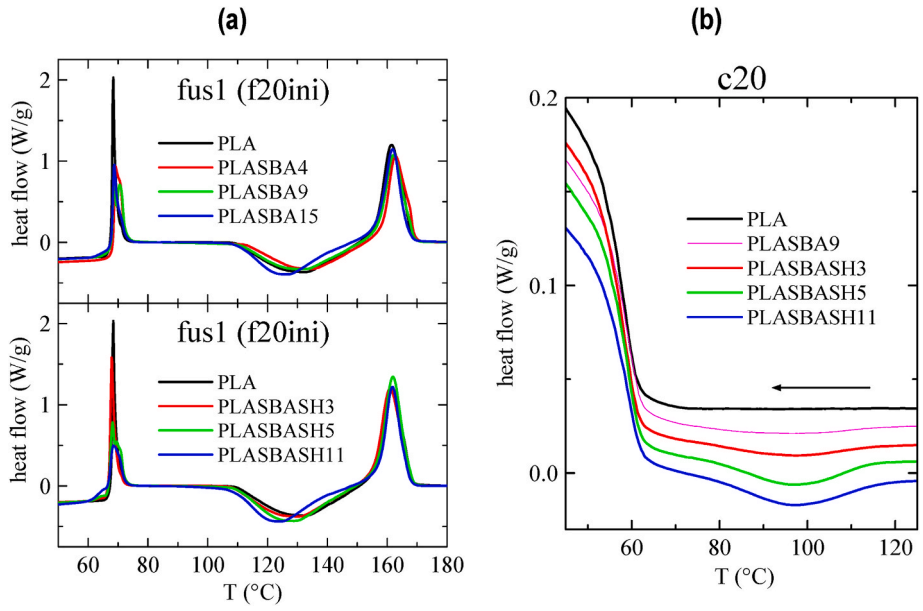

Fig. 5. (a) DSC heating curves (endo up) carried out at 20 °C/min for the PLA and its composites with SBA-15 (top) and SBASH (bottom) particles, during the first heating; (b) amplified DSC cooling curves (endo up) carried out from the melt at 20 °C/min for the neat PLA and its composites with SBASH. PLASBA9 composite is also included for comparison.

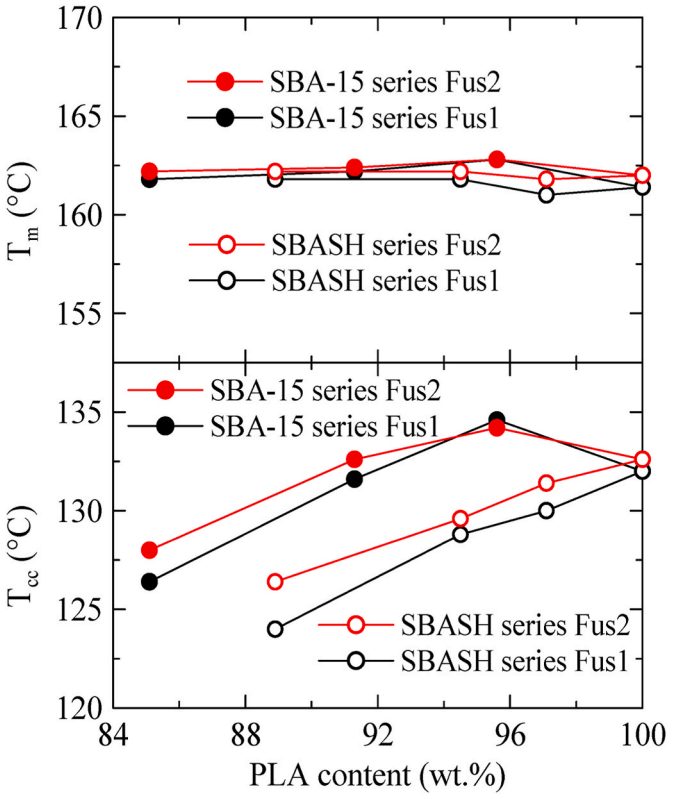

Fig. 6. Variation with the actual PLA content in the sample of the melting temperature (top) and of the cold crystallization temperature (bottom) for PLA and its composites with SBA-15 and SBASH, during the first (Fus1) and second heating (Fus2) process.

2.4. Obtainment of films

These composites were subsequently processed by compression molding in a hot-plate Collin press. Initially, the material was maintained at a temperature of 195 °C and at a pressure of 30 bar for 6 min. Afterwards, a cooling process was applied at the relatively rapid rate of around 80 °C/min and at a pressure of 30 bar to the different composites from their molten state to room temperature. These original compression-molded films were totally amorphous, as shown below.

On one hand, the three composites prepared using neat SBA-15 particles contain an amount in mesoporous silica of 4.4, 8.7 and 14.9 wt%, as determined by TGA, being then named as PLASBA4, PLASBA9 and PLASBA15, respectively. On the other hand, the three composites incorporating hybrid SBASH particles show a content in the inorganic component of 2.9, 5.4 and 11.1 wt%, being these materials designated as PLASBASH3, PLASBASH5 and PLASBASH11, respectively.

2.5. Scanning electron microscopy

Morphological details of the mesoporous SBA-15 particles, either pristine or containing the SH group, and the particles distribution in the samples were obtained by high resolution field emission scanning electron microscopy (FESEM), carried out in a S-8000 Hitachi equipment at room temperature in different cryo-fractured sections of composites at distinct mesoporous contents. Those thin sections of around 30 nm were cut by cryo-ultramicrotomy (Leica EM UC6) at −120 °C and deposited in a square mesh copper gride (CF-400-Cu, Ted Tella Inc.).

2.6. Thermogravimetric analysis

Thermogravimetric analysis (TGA) was performed in a TGA2 equipment of METLER TOLEDO under nitrogen and air atmospheres at a heating rate of 10 °C/min from 30 to 800 °C. Degradation temperatures of the distinct materials are determined as well as the SBA-15 amount incorporated into the composites, which has been estimated as an average of values obtained from the two environments (see below).

2.7. Differential Scanning Calorimetry

Calorimetric analyses were carried out in a TA Instruments Q100 calorimeter connected to a cooling system and calibrated with different standards. The sample weights were around 3 mg. A temperature interval from −30 to 180 °C was studied at a heating rate of 20 °C/min.

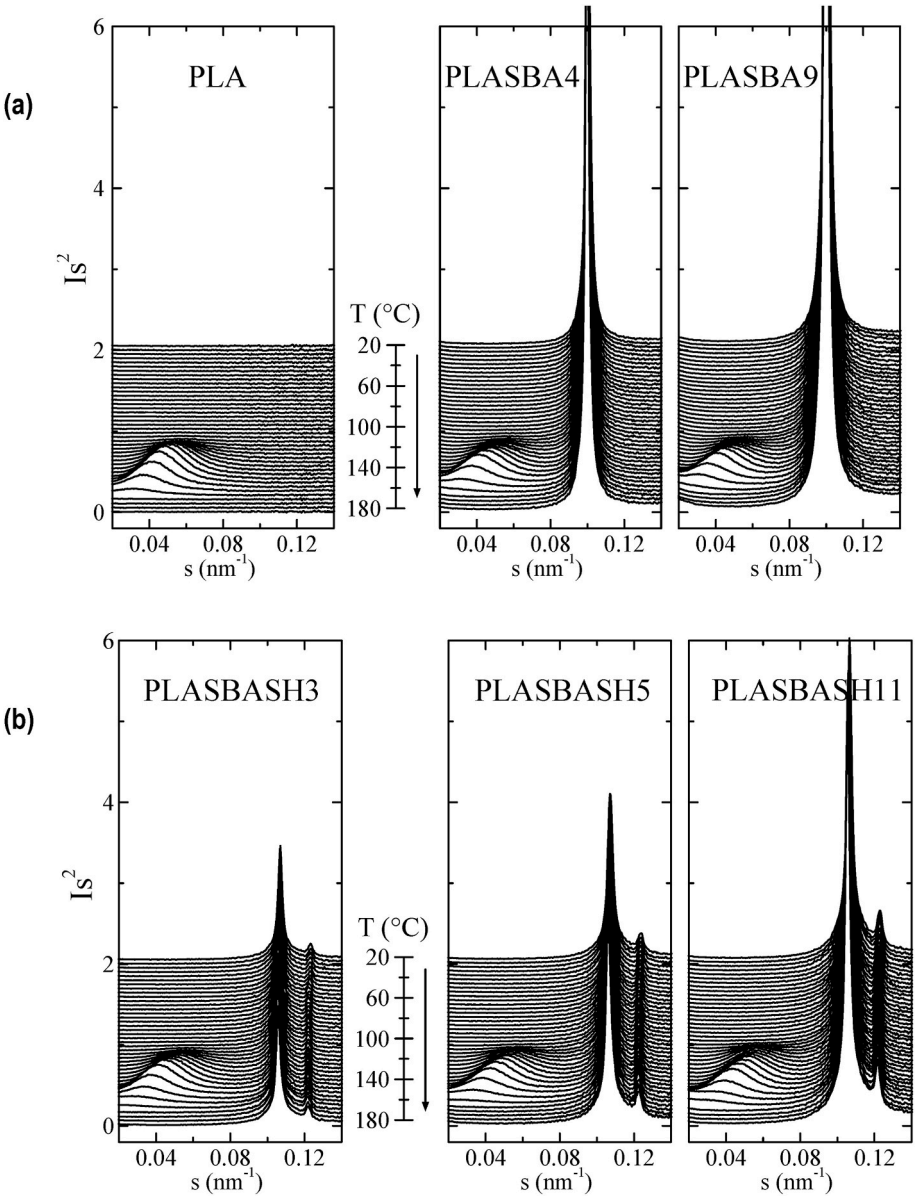

Fig. 7. Lorentz-corrected SAXS profiles for PLA and the composites with SBA-15 (a) and for the materials incorporating SBASH particles (b) during the first heating at 20 °C/min. Only one out of every two frames is plotted, for clarity.

Crystallinity degree from these calorimetric experiments was determined according to the following equation (1):

$$f_c^{norm\ PLA\ content} = \frac{(\Delta H_m - \Delta H_{cc})}{\Delta H_0 \times X_{PLA}} \quad (1)$$

where ΔH_m and ΔH_{cc} refer to the melting and cold crystallization enthalpies, respectively, of the composites during the heating run; ΔH_0 refers to the enthalpy of fusion of a perfectly PLA crystalline material, which is 93.1 J/g [43,44]; and X_{PLA} refers to the weight ratio of PLA in the composites.

2.8. X-ray experiments with conventional and synchrotron radiation

Wide angle X-Ray Diffraction (WAXD) patterns were recorded for characterizing neat and functionalized SBA-15 particles at room temperature in the reflection mode by using a Bruker D8 Advance diffractometer provided with a PSD Vantec detector (from Bruker, Madison, Wisconsin). Cu Kα radiation (λ = 0.15418 nm) was used, operating at 40 kV and 40 mA. The parallel beam optics was adjusted by a parabolic Göbel mirror with horizontal grazing incidence Soller slit of 0.12° and LiF monochromator. The equipment was calibrated with different standards. A step scanning mode was employed for the detector. The diffraction scans were collected with a 2θ step of 0.024° and 0.2 s per step.

Real-time variable-temperature simultaneous SAXS/WAXS experiments were carried out with synchrotron radiation in beamline BL11-NCD-SWEET at ALBA (Cerdanyola del Vallès, Barcelona, Spain) at a fixed wavelength of 0.1 nm. A Pilatus detector has been used for SAXS (off beam, at a distance of 296 cm from sample) and a Rayonix one for WAXS (at about 14.6 cm from sample, and a tilt angle of around 29°). A Linkam Unit, connected to a cooling system of liquid nitrogen, was employed for the temperature control. The calibration of spacings was obtained by means of silver behenate and Cr_2O_3 standards. The initial 2D X-ray images were converted into 1D diffractograms, as function of the inverse scattering vector, $s = 1/d = 2 \sin \theta/\lambda$, by means of pyFAI python code (ESRF), modified by ALBA beamline staff. Film samples, of around 5 × 5 × 0.1 mm, were used in the synchrotron analysis.

The X-ray crystallinity from WAXS profiles was assessed as the ratio

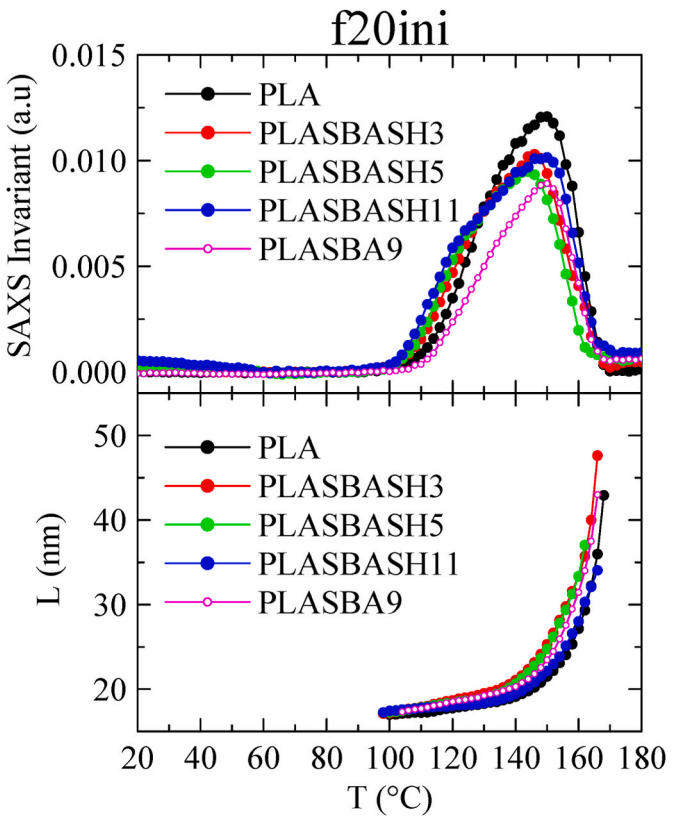

Fig. 8. Variation with temperature of the SAXS relative invariant (top) and of the long spacing (bottom) for the PLA and its composites with SBASH during the first heating at 20 °C/min. The values for PLASBA9 are also included, for comparison.

of normalized areas of the crystalline peaks and the total area of the background-corrected diffraction profile, by means of equation (2) [45]:

$$f_c{}^{NORM}{}_{WAXS} = \frac{A_{crystalline}{}^{NORMALIZED}}{A_{TOTAL}{}^{NORMALIZED}} = \frac{A_{crystalline}{}^{NORMALIZED}}{A_{amorphous}{}^{NORMALIZED} + A_{crystalline}{}^{NORMALIZED}} \quad (2)$$

where $A_{crystalline}^{NORMALIZED}$ is the normalized area of the crystalline reflections; $A_{TOTAL}^{NORMALIZED}$ is the normalized total area of the background-corrected diffraction profile; and, $A_{amorphous}^{NORMALIZED}$ is the normalized scattering area of the amorphous halo. Area of pure crystalline peaks was attained from the normalized area of total diffraction profile after subtracting the normalized scattering area of the amorphous halo, to which a coefficient was applied in order to achieve the perfect fit at the beginning and the end of the interval considered in each experimental profile [45]. This amorphous halo is taken from the X-ray pattern of a fully amorphous sample, obtained from the compression-molded films prepared at high cooling rates from the molten state.

2.9. Microhardness

A Vickers indentor attached to a Leitz microhardness tester was used to perform microindentation measurements undertaken at 23 °C. A contact load of 0.98 N and a time of 25 s were employed. Microhardness, MH, value (in MPa) was calculated according to the relationship [46,47]:

$$MH = 2\sin 68^{\circ}\left(\frac{P}{d^2}\right) \quad (3)$$

where P (in N) is the contact load and d (in mm) is the diagonal length of the projected indentation area. Diagonals were measured in the reflected light mode within 30 s of load removal, using a digital eyepiece equipped with a Leitz computer-counter-printer (RZA-DO).

3. Results and discussion

3.1. Characteristics of the SBA-15 and SBASH particles

Fig. 1 shows the FESEM images for the synthesized mesoporous silicas; neat SBA-15 (a) and hybrid SBASH (b) particles, respectively, as well as their corresponding X-ray diffractograms. FESEM pictures show the characteristic morphology of these mesoporous silicas consisting in interior nanometric channels, which are ordered in a hexagonal arrangement, although particles exhibit micrometric size. The border of the hybrid SBASH particles (Fig. 1b) appears to be more irregular, maybe because of the presence of mercaptopropyl group. The influence of this group in the mesoporous structure of the silica is also noticeable in the X-ray profiles, represented in Fig. 1c. Thus, the three main diffraction peaks (100), (110) and (200) [22] associated with the hexagonal ordering characteristic of neat SBA-15 silica, appear in order of increasing angles, as expected. On the contrary, diffractions (110) and (200) become less evident for the hybrid SBASH particles, pointing out that regularity of their ordered nanometric structure has been damaged by effect of the functionalization. Furthermore, the main (100) reflection is shifted to lower angle, meaning a greater size of pores in this decorated SBASH silica.

A loss of regularity has been also reported by other authors when including different groups in the mesoporous silica. The changes in the hexagonal arrangement are not very significant when modifying silica particles with metals or metal oxides [25–27,48]. In a previous study where mesoporous silica was decorated with silver, the mesoporosity was maintained after Ag incorporation but the results also showed that the order was somewhat decreased [49].

In other cases, the loss of ordering was, however, very important when bulky molecules are used for modification of the SBA-15 silica, similar to what is noted in this present work when mercaptopropyl groups are incorporated in the structure. Besides this insertion of different molecules, loss of regularity can also occur for other reasons; for example, hydrothermal treatment [50].

Thermogravimetric analysis (TGA) curves and their corresponding derivatives under 2 atm, inert and oxidative, are represented in Fig. 2 for these SBA-15 and SBASH particles. Differences between them are deduced from these curves. A weight loss is observed in the interval from around 70 to 100 °C in both atmospheres for SBA-15, which is associated with elimination of adsorbed water. A similar reduction in weight is also noted in SBASH particles in the same temperature range, since these particles are enabled to adsorb water from the environment. At higher temperatures and distinctively to what the SBA-15 particles exhibit, a considerable loss of weight is noticed in this SBASH silica, in both inert and oxidative atmospheres. This decomposition step is ascribed to the mercaptopropyl group degradation. The process occurs at 362 °C under an inert medium while it is shifted to lower temperatures, at 270 °C, under oxidative conditions, because oxygen assists the mercaptopropyl group decomposition.

TGA experiments allow also determining the content of the organic loading in the particles from the mass left at temperatures above 700 °C. This approach has been used in literature for estimation of the amount of -SH groups. Furthermore, other techniques, such as X-ray photoelectron spectroscopy (XPS), solid-state nuclear magnetic resonance (NMR) or energy-dispersive X-ray spectroscopy (EDX) are employed complementarily for analyzing presence of these groups and other different characteristics of these decorated silicas [51–54]. In the present investigation, the silica content in the modified SBASH particles was 63.7 wt%, determined from these TGA curves, so the amount in mercaptopropyl groups inside the particles is about 33.2 wt% (after the subtraction of the adsorbed water, which was in a percentage of around 3.1 wt%). It should be commented that adsorption of water is very easy

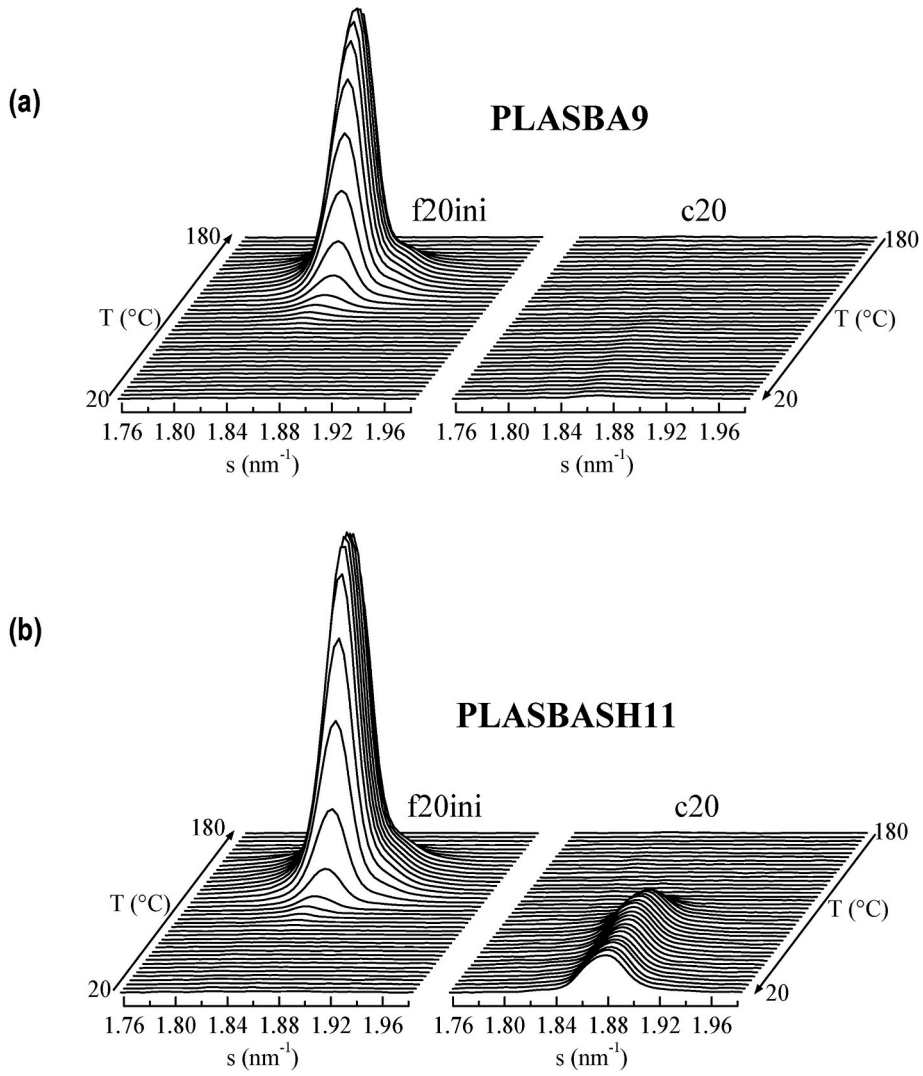

Fig. 9. Synchrotron WAXS profiles, in the region of the main (110/200) PLA diffraction, for composites PLASBA9 **(a)** and PLASBASH11 **(b)** during the first heating at 20 °C/min (left plots) and the subsequent cooling at 20 °C/min (right plots). Only one out of every two frames is plotted, for clarity.

and common in silicas. Consequently, appropriate drying protocols have to be applied before their use (see Experimental). Taken into consideration that silica particles (either neat or pristine ones) will be the minor component in the PLA based composites, it is interesting that amount of mercaptopropyl groups is relatively significant to play a role in the final materials.

3.2. Morphological details of composites with SBA-15 and SBASH

Fig. 3 displays the FESEM images of the PLA composites containing the highest content in SBA-15 or SBASH silica, i.e., PLASBA15 and PLASBASH11, respectively. These photographs allow deducing that both silicas are rather well distributed within the PLA matrix. In addition to this quite uniform dispersion, formation of particles agglomerates with large dimensions is not observed. Thus, the protocol used along preparation of these composites, including the last stage of compression molding to prevent solvent residues, is appropriate for obtaining suitable biobased PLA composites.

Incorporation of mercaptopropyl groups in the SBA-15 silica through a one-pot synthetic approach seems to lead to a better particle distribution in the PLASBASH11 composite compared with the PLASBA15 material. As aforementioned, compatibility between polymers and mesoporous silica, as SBA-15, is usually not good owing to their chemical differences. Addition of the mercaptopropyl groups into the silica appears to boost better interactions with PLA through the organic chains now linked to the silica. Physical interactions between PLA ester groups and those SHs existing in the mercaptopropyl compound can be developed.

3.3. Thermal stability of the different composites

Fig. 4 shows the TGA curves for the different PLA composites with SBA-15 or SBASH particles under nitrogen (left plots) and under air (right plots). Both inert and oxidative decompositions occur through a unique stage, although temperatures of their beginning are slightly different, depending on the type of atmosphere. Thus, decomposition starts at around 315 °C under a nitrogen medium and at about 300 °C in air (finishing in both cases at about 400 °C).

The PLA decomposition process with commercial SBA-15 composites was previously studied by our group in different publications [40,42,45]. Now, the composites based on PLA contain particles of SBA-15 and of SBA-15 modified with mercaptopropyl groups that has been synthesized in the laboratory. These composites, similar to what was observed in those using commercial SBA-15, show a slightly higher thermal stability than the neat PLA (see Table 1). Incorporation of hybrid silica particles with mercaptopropyl groups does not alter the thermal stability

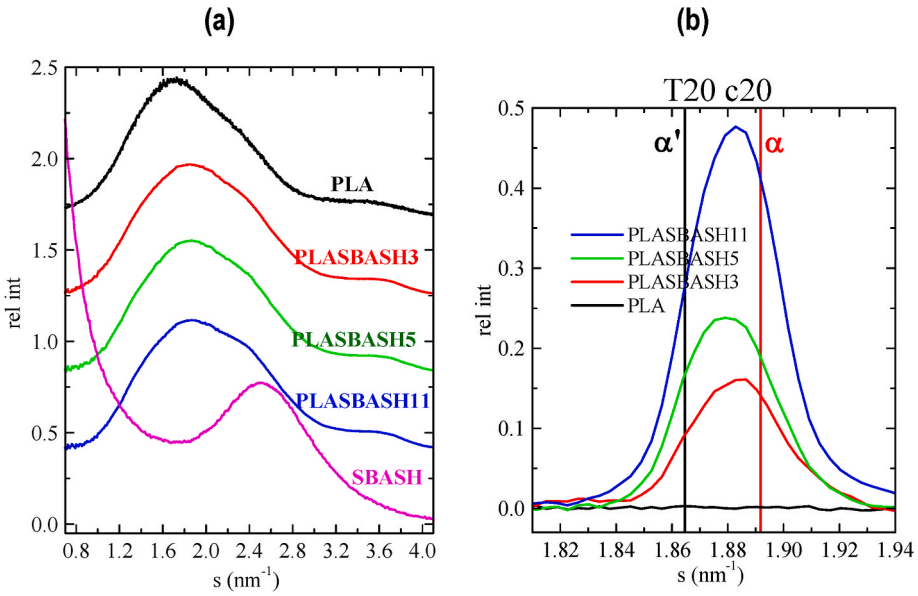

Fig. 10. (a) WAXS profiles, at room temperature, of the initial compression-molded samples for neat PLA and its composites with SBASH, together with the one for the original SBASH particles; (b) amplified room-temperature WAXS profiles, in the region of the main (110/200) diffraction, for the PLA and its composites with SBASH after cooling from the melt at 20 °C/min.

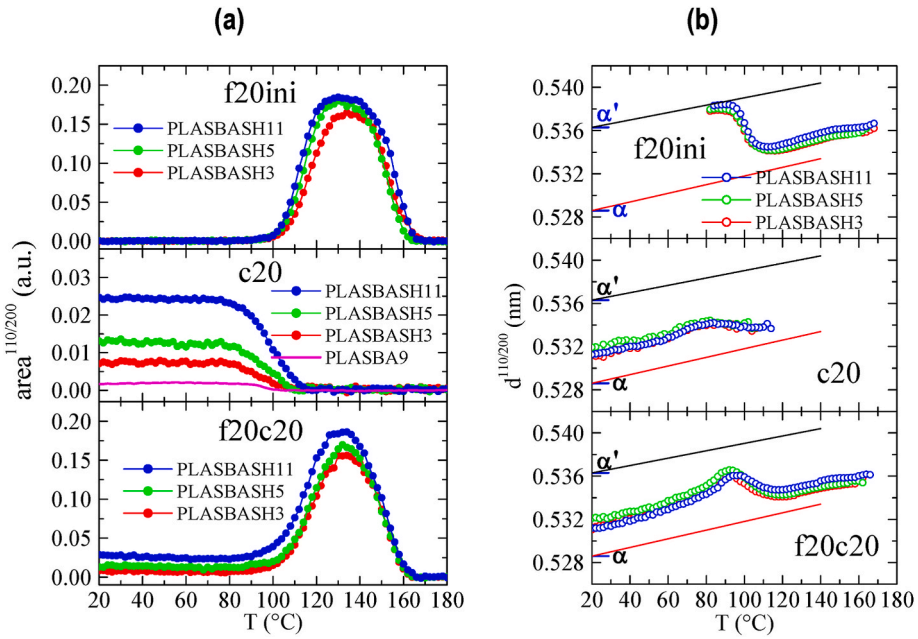

Fig. 11. Variation with temperature of: (a) the area, and (b) the spacing of the main (110/200) PLA diffraction, for the composites of PLA with SBASH silica during the first heating (f20ini), cooling (c20) and second heating (f20c20). Note that the cooling experiments in (a) are amplified by a factor of 6. The behavior of a sample of PLASBA9 is included for comparison in these c20 runs. The lines in (b) represent the variation with temperature of the spacings for the pure α′ and α polymorphs [36].

of the resulting composites. Consequently, there is not modification in the degradation sequence for any of the 2 atm evaluated.

Moreover, the actual silica content in the composites can be deduced from these TGA measurements. Results reported in Table 1 correspond to those obtained as the average found for the 2 atm. Furthermore, Table 1 also lists the temperature at the maximum in the DTGA curves (T_{max}^{DTGA}) for the PLA composites either with SBA-15 or SBASH silica under air and under nitrogen environments.

3.4. Thermal transitions by DSC

Fig. 5a shows the DSC curves, carried out at 20 °C/min, for neat PLA and its composites with SBA-15 (top) and SBASH (bottom) during the first heating runs, while the amplified cooling curves are presented in Fig. 5b. Several phase transitions can be observed in the heating curves in order of increasing temperatures: glass transition, cold crystallization and melting endotherm. For the first heating, it is important to mention that the total enthalpy involved in the entire DSC curve is practically zero for all of the samples, indicating that the initial compression-molded materials are completely amorphous, independently of the

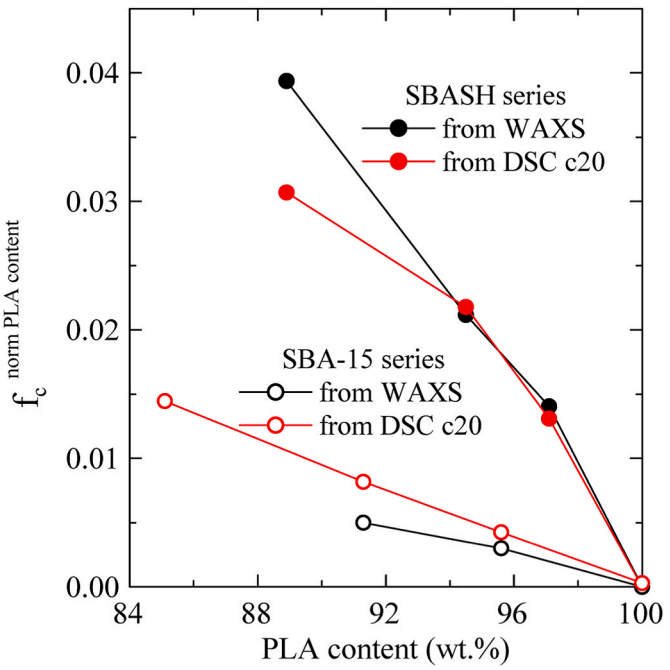

Fig. 12. Variation with the actual PLA content in the composite of the crystallinity (normalized to the PLA content) estimated from either WAXS or from DSC, for the PLA and its composites with either SBA-15 or SBASH particles after the cooling from the melt at 20 °C/min.

composition in pristine or hybrid silica particles. Regarding the glass transition, T_g, these first heating curves show a prominent peak arising from the physical aging of the samples when standing at room temperature. Since the samples have been for a long time at room temperature (varying from around 15 to 30 °C), the physical aging peak appears split in some of the samples.

At higher temperatures, a cold crystallization is observed in all cases, with a temperature, T_{cc}, which is inferior in all of the composites incorporating SBASH particles in relation to the neat PLA, and presenting lower values as the silica content increases. However, in the PLA materials with neat SBA-15 silica, only PLASBA15 is showing a value significantly smaller than that exhibited by the pure PLA matrix. These results indicate an important nucleation effect of the SBASH silica while that for the pristine SBA-15 is inferior, pointing out better interactions at surfaces between the two constituents, polymer and SBASH, of the composites when the particles have been functionalized (as quantified below).

The phase transition at higher temperatures refers to the melting endotherm. Typically, this endotherm shows two clear components in PLA samples when the scanning rate is 10 °C/min [26,42], the lower temperature one being ascribed to the true melting temperature of the initial crystals, and the second one arising from a recrystallization process occurred on melting. In the present case, however, a heating rate of 20 °C/min has been chosen, in order to match the one used in the real-time variable-temperature synchrotron experiments (see below). With this heating rate, the melting endotherms (either in the first or in the second melting) do not show two well separated components, although a shoulder in the high-temperature side is observed.

Regarding the cooling from the melt, the amplified cooling curves can be seen in Fig. 5b. Importantly, neat PLA does not crystallize at all on cooling from the melt at 20 °C/min, a fact that has been shown before [26,42]. On the contrary, a relatively small but clear crystallization exotherm is observed for the composites, which is really small for PLASBA9, being even greater in the composite PLASBASH3, containing a much lower amount in silica compared with the PLASBA9. Furthermore, crystallization in the set of composites with the functionalized silica increases considerably with the SBASH content, pointing out a substantial nucleation effect of SBASH silica in the ordering of PLA and the importance of the superficial properties of these decorated particles to boost crystallization even at this high cooling rate.

The variation with the actual PLA content in the sample of the melting temperature and of the cold crystallization temperature for neat PLA and its composites with either SBA-15 or SBASH, during the first and second melting, is displayed in Fig. 6. It can be observed that all values of T_m for both the first and second heating experiments are practically inside the experimental error, considered to be around ±1 °C. Furthermore, T_m is rather independent of absence or presence of silica particles, (either neat or functionalized ones), and of their content.

On the contrary, T_{cc} shows a clear variation: for the SBA-15 composites it rises somewhat on passing from PLA to PLASBA4, and it decreases at higher silica contents. For the SBASH composites, T_{cc} shows, however, a continuous and significant decrease with increasing content of SBASH particles, indicating a nucleation ability of the SBASH silica much higher than the one exhibited by neat SBA-15 particles. That effect could be associated with the presence of the mercaptopropyl groups in these composites and their stronger interaction with PLA chains due to their superficial features, as aforementioned, thus improving even more the nucleation effect shown by SBA-15.

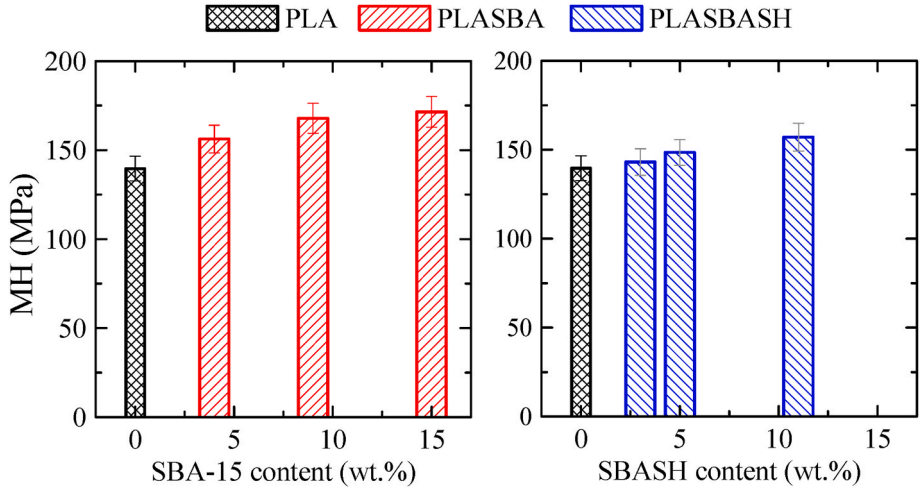

Fig. 13. Microhardness, MH, dependence on mesoporous silica content for the different composites.

3.5. Crystalline features in the composites of PLA with SBA-15 and SBASH

Real-time variable temperature synchrotron experiments have been performed on selected samples in order to learn about different crystalline features in these composites. Fig. 7 shows the Lorentz-corrected SAXS profiles for the PLA composites with SBA-15 and SBASH silicas during the first heating run at 20 °C/min. Two clear regions can be deduced from these diffractograms. Firstly, the main SAXS diffractions of the silicas appear in the region at the highest values of scattering vector *s*, above 0.09 nm^{-1}. For the composites with pristine SBA-15 particles, a rather narrow and intense peak is observed at *s* around 0.100 nm^{-1} (spacing of 10.0 nm). In the composites with hybrid SBASH silica, however, a split peak is observed with the main component at *s* around 0.106 nm^{-1} (spacing of 9.43 nm), while a smaller peak is observed at *s* around 0.122 nm^{-1} (spacing of 8.20 nm). This result confirms the reduction of regularity, mentioned above, which may occur when functionalizing the mesoporous silicas.

Moreover, long spacing of PLA is observed in the second region of Fig. 7, at lower *s* values. This long spacing does not appear at room temperature, owing to the amorphous nature shown by the initial specimens. Only after the cold crystallization the long spacing is clearly observed, shifting to lower *s* values (higher spacings) as the temperature increases, until its disappearance when the sample melts. In fact, Fig. 8 presents the variation with temperature of the SAXS relative invariant [55,56] and of the long spacing for neat PLA and its composites with SBASH during the first heating at 20 °C/min, with the values for PLASBA9 also included, for comparison. Not very relevant differences are observed in those two parameters among the different samples, except for the mentioned appearance of the cold crystallization at lower temperatures as the content in SBASH particles increases, indicating the favorable role that mercaptopropyl groups play in promoting PLA three-dimensional ordering ascribed to more satisfactory interactions between modified silica and polymeric matrix. And, obviously, the long spacing is not observed until that cold crystallization occurs. Moreover, the long spacing values decrease first in PLASBASH3 and PLASBASH5 in relation to neat PLA, while the values for PLASBASH11 show an increase in such a way that now the long spacing is similar to that of PLA. In summary, it has been deduced that although the mercaptopropyl groups improved the nucleation capacity, the size of the crystals is rather similar in all samples, including neat PLA.

Coming back to the SAXS invariant, a further inspection seems to indicate higher values at the maximum for PLA. This is not really true, since these values have not been corrected for the actual PLA content in the sample.

Additional information about the crystalline features in these composites is deduced from the WAXS diffractograms. Thus, Fig. 9 shows the synchrotron WAXS profiles, in the region of the main (110/200) PLA diffraction, for the composites PLASBA9 and PLASBASH11 during their first heating at 20 °C/min (left plots) and the subsequent cooling at 20 °C/min (right plots). It can be observed for the former that the first diffractograms, corresponding to the initial compression-molded samples, do not show the crystalline (110/200) diffraction, *i.e.*, these two composites (and all the other ones) are completely amorphous as well as the rest of materials independently of type of silica incorporated and of its content (profiles not shown). On increasing temperature, the cold crystallization takes place first, followed later by the final melting of the sample. During the subsequent cooling from the melt (right plots in Fig. 9a and b), the crystallization is noticed for composite PLASBASH11 at a temperature around 100 °C. The most relevant feature is, however, that this (110/200) diffraction peak shows a maximum intensity which is only around 6 times smaller than the maximum observed after the cold crystallization in the first heating. It means, therefore, that a cooling rate of 20 °C/min is enough to develop a significant amount of crystallinity in this PLASBASH11 composite. On the contrary, a much smaller intensity is observed for that (110/200) diffraction peak in composite PLASBA9. All these diffractograms in Fig. 9 will be further analyzed below.

Fig. 10a exhibits the amplified WAXD diffractograms, at room temperature, of the initial compression-molded samples for the PLA and its composites with SBASH. As mentioned above, all the initial specimens appear to be amorphous, and this aspect is clearly ascertained from this figure, since the different samples show only an amorphous-like wide profile, with no sign of crystallinity. The only difference among the samples is the high-angle component of the main peak, with an increasing contribution as the content in SBASH silica increases. This is due to the fact that SBASH particles are also amorphous, like neat SBA-15 ones [34], at short range and present a peak centered in that region, as seen in the lower diffractogram of Fig. 10a.

Fig. 10b presents the amplified room-temperature WAXS profiles, in the region of the main (110/200) diffraction, for the PLA and its composites with SBASH after the cooling from the melt at 20 °C/min. As mentioned above, neat PLA is not able to crystallize when cooling at that rate. On the contrary, and in agreement with Fig. 4b, a significant (although relatively small) diffraction peak is observed for the composites (this fact has been also ascertained above when commenting Fig. 9 for composites PLASBA9 and PLASBASH11), whose intensity becomes higher with rising SBASH amount in the composite. Thus, crystallinity after cooling from the melt at 20 °C/min increases substantially as the SBASH content is raised, as seen from Fig. 10b. Moreover, that main diffraction appears centered at spacings in between those reported for the pure α′ and α polymorphs [57].

The variation with temperature of the area of the main (110/200) PLA diffraction for the composites of PLA with SBASH silica during the first heating (f20ini), cooling (c20) and second heating (f20c20), can be seen in Fig. 11a. For the first heating, the area is initially zero until the occurrence of the cold crystallization, where the area increases steeply, the more as the content of decorated silica is higher, reaching a maximum and decreasing again to zero during melting, as mentioned above. In the subsequent cooling experiments, the area increases, depending on the amount of SBASH particles, during crystallization in the samples, although it takes place in a small extent. Note that the C20 experiments in the middle plot of Fig. 11a are amplified by a factor of 6. It is clearly observed that the degree of crystallization increases with the SBASH content in the composite. Moreover, the behavior of a sample of PLASBA9 is included for comparison in these cooling experiments, showing considerably lower values of the area (and, consequently, of the crystallinity reached). These results once again demonstrate the importance of having decorated the silica particles and having modified their surface characteristics to favor their nucleating effect in the PLA matrix. These values are quantified below.

Regarding the results for the second heating, the lower plot in Fig. 11a shows an initial small area, developed in the prior cooling from the melt, which depends on the SBASH content in the composite, and at higher temperature the cold crystallization (of the remaining polymer segments not crystallized during the previous cooling) is observed.

Fig. 12 depicts the variation as a function of this PLA content of the crystallinity normalized to the actual PLA content in the composite. The crystallinity can be determined by equation (2) from the diffractograms like those in Fig. 9 by subtracting the corresponding amount of amorphous component [45], this component being represented in Fig. 10a. The crystallinity estimated from WAXS is compared in Fig. 12 with the one deduced from DSC, determined by equation (1), for the PLA and its composites with either SBA-15 or SBASH particles after the cooling from the melt at 20 °C/min. A fairly good agreement, especially for the lower silica contents, is observed between the DSC and WAXS results. It is important to note that rather small degrees of crystallinity are involved (lower than 4 %). Anyway, the nucleation ability of SBASH for the crystallization of PLA is well evident, which, in fact, is considerably higher than the one found in the PLASBA composites, which show crystallinity values around 4 times smaller than those for the PLASBASH composites. At this point, it should be taken into account that the cooling conditions applied in this study (a rate of 20 °C/min) are not the most

favorable ones considering the deficient PLA crystallization. Thus, differences between the nucleation capability of the SBASH compared with that shown by the SBA-15 particles could be greater if crystallization protocol was more satisfactory, i.e., performed at lower rates.

The variation of other important parameter of the (110/200) PLA diffraction, the spacing, is plotted in Fig. 11b as function of temperature, during the first heating, cooling and second heating, for the three SBASH composites. In the first heating, the spacing shows up after the cold crystallization of the samples, meaning that they are initially amorphous. The lines in Fig. 11b represent the estimated variation with temperature of the spacings for the pure α′ and α polymorphs, based on the results reported before [45]. It can be observed that immediately after the beginning of the cold crystallization (at around 80 °C), the samples crystallize initially under the disordered α′ modification, but the transformation from α′ to α polymorph occurs at a slightly higher temperature, centered at around 100 °C. In fact, the pure α modification is not totally reached, as deduced from Fig. 11b, top plot. Regarding the subsequent cooling, the spacings are now in between those of the two modifications, fact already deduced from Fig. 10b for the room-temperature values.

The behavior of the second heating (lower plot in Fig. 11b) is somewhat more complicated. Since a small crystallinity was already developed in the prior cooling, now the cold crystallization of the remaining not-crystallized segments shows up, and as happened in the first melting, the cold crystallization first leads to spacings closer to the pure disordered α′ polymorph, but the α'→α transformation occurs at higher temperatures, and the structure is much closer to the ordered α modification.

3.6. Mechanical behavior of the different composites

Microhardness (MH) measurements performed at room temperature on the compressed-molded films provides information about the mechanical behavior exhibited by these two PLA composites families. As previously mentioned, all of them are amorphous. Fig. 13 shows the MH values of all studied composites as a function of the silica content. On the left graph, composites with SBA-15 display an increase of MH with silica content, from 139.6 MPa for PLA to 171.5 MPa for PLASBA15. This fact points out the reinforcement role that silica particles exert in the amorphous glassy PLA matrix. This tendency is expected because the SBA-15 silica is a component harder than polymeric chains.

An analogous increasing behavior is observed as function of silica content in composites incorporating the SBASH particles, but in a less extent. The highest MH value is 157.0 MPa for PLASBASH11, 10.9 MPa lower than that attained in PLASBA9 (167.9 MPa), which is the composite with neat SBA-15 at similar content. Functionalization of SBA-15 silica with mercaptopropyl groups attempts to change characteristics at particle surface to boost silica-PLA interactions and, consequently, to lead to an improvement in distributing the inorganic component within the PLA matrix as well as in the PLA nucleation ability during its crystallization. Both purposes have been reached but decoration has anchored mercaptopropyl groups into the hybrid silica, becoming softer than the neat SBA-15 particles, and has triggered the loss of ordering in the resultant SBASH particles compared with that shown by pristine SBA-15 silica. These two facts seem to have affected the final hardness of the SBASH particles in such a way that its reinforcement effect on the resulting PLASBASH composites is not as high as that provided by the neat SBA-15 in its corresponding PLASBA materials. Accordingly, MH increases as content of hybrid silica does, but these PLASBASH composites show lower values than those exhibited by the PLASBA materials, although MH in both sets is higher than the one observed for pristine PLA.

4. Conclusions

Functionalization of SBA-15 with mercaptopropyl groups (SBASH particles) is performed following a one-pot synthetic protocol. These modified particles show the characteristic hexagonal arrangement of SBA-15 silica, although a reduction of its ordering is observed. Afterwards, neat and decorated silicas have been incorporated into PLA and several composites are prepared by solvent casting, followed by compression molding applying a rapid cooling from the melt.

A better particle dispersion is noticed in the composites incorporating the SBASH silica, indicating that presence of these mercaptopropyl groups in the hybrid silica leads to a better interaction with the PLA matrix. Furthermore, an important nucleation effect of decorated SBASH in the crystallization of PLA is found, being deduced from location of the cold crystallization temperature and from the degree of crystallinity. Otherwise, long spacings are rather similar for all the different composites and for the neat PLA. Thus, the size of the crystals is rather similar in all samples analyzed, although the mercaptopropyl groups improved the nucleation capacity of PLA.

An increase in microhardness is observed in all composites compared to pure PLA, highlighting the reinforcing role played by silica particles. This increase is greater in PLASBA composites than in PLASBASH, because the presence of mercaptopropyl groups softens the hybrid silica particles as well as reducing their characteristic ordering.

All these findings indicate that the protocols used for the preparation of functionalized SBASH silica and the subsequent obtainment of their composites with PLA are appropriate for attaining suitable biobased PLA composites with some improved performances.

CRediT authorship contribution statement

Tamara M. Díez-Rodríguez: Writing – review & editing, Writing – original draft, Methodology, Investigation, Formal analysis, Data curation. **Enrique Blázquez-Blázquez:** Writing – review & editing, Investigation, Formal analysis. **João P. Lourenço:** Writing – review & editing, Methodology, Investigation. **Juan C. Martínez:** Writing – review & editing, Methodology. **María L. Cerrada:** Writing – review & editing, Writing – original draft, Supervision, Project administration, Methodology, Investigation, Funding acquisition, Conceptualization. **Ernesto Pérez:** Writing – review & editing, Writing – original draft, Supervision, Investigation, Funding acquisition, Formal analysis, Data curation.

Declaration of competing interest

The authors declare that they have no known competing financial interests or personal relationships that could have appeared to influence the work reported in this paper.

Acknowledgments

This research was funded by MCIN/AEI/10.13039/501100011033, grant number PID2020-114930 GB-I00. JPL thanks Portuguese FCT for funding (Project UIDB/00100/2020). Authors are grateful to the Characterization Service at ICTP-CSIC for FESEM, TGA and X-ray diffraction facilities as well as to its personnel for support. The synchrotron experiments were carried out in the beamline BL11-NCD-SWEET at the ALBA Synchrotron Light Facility with the collaboration of ALBA staff, to whom the authors are grateful for their support.

Data availability

Data will be made available on request.

References

[1] D. Garlotta, J. Polym. Environ. 9 (2001) 63–84, https://doi.org/10.1023/A:1020200822435.
[2] A. Sodergard, M. Stolt, Prog. Polym. Sci. 27 (2002) 1123–1163, https://doi.org/10.1016/S0079-6700(02)00012-6.

[3] R. Auras, B. Harte, S. Selke, Macromol. Biosci. 4 (2004) 835–864, https://doi.org/10.1002/mabi.200400043.
[4] R. Mehta, V. Kumar, H. Bhunia, S.N. Upadhyay, J. Macromol. Sci., Part C 45 (2005) 325–349, https://doi.org/10.1080/15321790500304148.
[5] N. Singh, O.A. Ogunseitan, M.H. Wong, Y. Tang, Sustainable Horizons 2 (2022) 100016, https://doi.org/10.1016/j.horiz.2022.100016.
[6] S. Saeidlou, M.A. Huneault, H. Li, C.B. Park, Prog. Polym. Sci. 37 (2012) 1657–1677, https://doi.org/10.1016/j.progpolymsci.2012.07.005.
[7] B. Zhu, Y. Wang, H. Liu, J. Ying, C. Liu, C. Shen, Compos. Sci. Technol. 190 (2020) 108048, https://doi.org/10.1016/j.compscitech.2020.108048.
[8] A. Zotti, S. Zuppolini, T. Tabi, M. Grasso, G. Ren, A. Borriello, M. Zarrelli, Composites, Part B 153 (2018) 364–375, https://doi.org/10.1016/j.compositesb.2018.08.128.
[9] W. Pivsa, S. Pivsa, J. Polym. Environ. 27 (2019) 1821–1827, https://doi.org/10.1007/s10924-019-01478-z.
[10] Y. Xia, S. Qian, W. Lu, Z. Zhang, H. Cheng, K. Sheng, Polym. Compos. 44 (2023) 8750–8765, https://doi.org/10.1002/pc.27734.
[11] I. Kvien, S.T. Bjom, K. Oksman, Biomacromolecules 6 (2005) 3160–3165, https://doi.org/10.1021/bm050479t.
[12] A. Pei, Q. Zhou, L.A. Berglund, Compos. Sci. Technol. 70 (2010) 815–821, https://doi.org/10.1016/j.compscitech.2010.01.018.
[13] J.-M. Raquez, Y. Murena, A.-L. Goffin, Y. Habibi, B. Ruelle, F. DeBuyl, P. Dubois, Compos. Sci. Technol. 72 (2012) 544–549, https://doi.org/10.1016/j.compscitech.2011.11.017.
[14] E. Rojo, M.V. Alonso, B. del Saz-Orozco, M. Oliet, F. Rodriguez, J. Appl. Polym. Sci. 132 (2015) 42157, https://doi.org/10.1002/app.42157.
[15] S. Saini, M.N. Belgacem, M.-C.B. Salon, J. Bras, Cellulose 23 (2016) 795–810, https://doi.org/10.1007/s10570-015-0854-1.
[16] S. Qian, K. Sheng, Compos. Sci. Technol. 148 (2017) 59–69, https://doi.org/10.1016/j.compscitech.2017.05.020.
[17] L. Xu, J. Zhao, S. Qian, X. Zhu, J. Takahashi, Compos. Sci. Technol. 203 (2021) 108613, https://doi.org/10.1016/j.compscitech.2020.108613.
[18] J. Tian, Z. Cao, S. Qian, Y. Xia, J. Zhang, Y. Kong, K. Sheng, Y. Zhang, Y. Wan, J. Takahashi, Nanotechnol. Rev. 11 (2022) 2469–2482, https://doi.org/10.1515/ntrev-2022-0142.
[19] S. Qian, Y. Kong, H. Cheng, S. Tu, C. Zhai, Surface. Interfac. 42 (2023) 103315, https://doi.org/10.1016/j.surfin.2023.103315.
[20] E. Blázquez-Blázquez, R. Barranco-García, T.M. Díez-Rodríguez, M.L. Cerrada, E. Pérez, Polymers 15 (2023) 624, https://doi.org/10.3390/polym15030624.
[21] J.S. Beck, J.C. Vartuli, W.J. Roth, M.E. Leonowicz, C.T. Kresge, K.D. Schmitt, C.T. W. Chu, D.H. Olson, E.W. Sheppard, S.B. McCullen, J.B. Higgins, J.L. Schlenker, J. Am. Chem. Soc. 114 (1992) 10834–10843, https://doi.org/10.1021/ja00053a020.
[22] D.Y. Zhao, J.L. Feng, Q.S. Huo, N. Melosh, G.H. Fredrickson, B.F. Chmelka, G. D. Stucky, Science 279 (1998) 548–552, https://doi.org/10.1126/science.279.5350.548.
[23] C.T. Kresge, M.E. Leonowicz, W.J. Roth, J.C. Vartuli, J.S. Beck, Nature 359 (1992) 710–712, https://doi.org/10.1038/359710a0.
[24] D. Zhao, Q. Huo, J. Feng, B.F. Chmelka, G.D. Stucky, J. Am. Chem. Soc. 120 (1998) 6024–6036, https://doi.org/10.1021/ja974025i.
[25] M.H. Huang, A. Choudrey, P. Yang, Chem. Commun. (2000) 1063–1064, https://doi.org/10.1039/B002549F.
[26] T.M. Díez-Rodríguez, E. Blázquez-Blázquez, M. Fernández-García, A. Muñoz-Bonilla, E. Pérez, M.L. Cerrada, Microporous Mesoporous Mater. 352 (2023) 112493, https://doi.org/10.1016/j.micromeso.2023.112493.
[27] S. Huang, C. Li, Z. Cheng, Y. Fan, P. Yang, C. Zhang, K. Yang, J. Lin, J. Colloid Interface Sci. 376 (2012) 312–321, https://doi.org/10.1016/j.jcis.2012.02.031.
[28] I.M. El-Nahhal, J.K. Salem, N.S. Tabasi, J. Sol. Gel Sci. Technol. 87 (2018) 647–656, https://doi.org/10.1007/s10971-018-4763-2.
[29] C.-H. Liu, N.-C. Lai, S.-C. Liou, M.-W. Chu, C.-H. Chen, C.-M. Yang, Microporous Mesoporous Mater. 179 (2013) 40–47, https://doi.org/10.1016/j.micromeso.2013.05.018.
[30] L.M. Wei, N.T. Hu, Y.F. Zhang, Materials 3 (2010) 4066–4079, https://doi.org/10.3390/ma3074066.
[31] X. Xu, Ch Song, J.M. Andrésen, B.G. Miller, A.W. Scaroni, Microporous Mesoporous Mater. 62 (2003) 29–45, https://doi.org/10.1016/S1387-1811(03)00388-3.
[32] X. Wang, X. Ma, Ch Song, D.R. Locke, S. Siefert, R.E. Winans, J. Möllmer, M. Lange, A. Möller, R. Gläser, Microporous Mesoporous Mater. 169 (2013) 103–111, https://doi.org/10.1016/j.micromeso.2012.09.023.
[33] A. de Sousa, E. Martins Barros de Sousa, R.G. de Sousa, J. Nanosci. Nanotechnol. 15 (2015) 9438–9448, https://doi.org/10.1166/jnn.2015.10489.
[34] R. Barranco-García, J.M. López-Majada, J.C. Martínez, J.M. Gómez-Elvira, E. Pérez, M.L. Cerrada, Microporous Mesoporous Mater. 272 (2018) 209–216, https://doi.org/10.1016/j.micromeso.2018.06.032.
[35] S.I.R. Castillo, S. Ouhajji, S. Fokker, B.H. Erné, C.T.W.M. Schneijdenberg, D.M. E. Thies-Weesie, A.P. Philipse, Microporous Mesoporous Mater. 195 (2014) 75–86, https://doi.org/10.1016/j.micromeso.2014.03.047.
[36] D. Niu, Z. Ma, Y. Li, J. Shi, J. Am. Chem. Soc. 132 (2010) 15144–15147, https://doi.org/10.1021/ja1070653.
[37] Y. Yang, N. Nakada, R. Nakajima, M. Yasojima, C. Wang, H. Tanaka, J. Hazard Mater. 244–245 (2013) 582–587, https://doi.org/10.1016/j.jhazmat.2012.10.056.
[38] R. Barranco-García, J.M. Gómez-Elvira, J.A. Ressia, L. Quinzani, E.M. Vallés, E. Pérez, M.L. Cerrada, Microporous Mesoporous Mater. 294 (2020) 109945, https://doi.org/10.1016/j.micromeso.2019.109945.
[39] T.M. Díez-Rodríguez, E. Blázquez-Blázquez, N.L.C. Antunes, M.R. Ribeiro, E. Pérez, M.L. Cerrada, J. Compos. Sci. 5 (2021) 321, https://doi.org/10.3390/jcs5120321.
[40] T.M. Díez-Rodríguez, E. Blázquez-Blázquez, E. Pérez, M.L. Cerrada, Polymers 14 (2022) 1237, https://doi.org/10.3390/polym14061237.
[41] A.E. Ferreira, M.L. Cerrada, E. Pérez, V. Lorenzo, H. Cramail, J.P. Lourenço, M. R. Ribeiro, Microporous Mesoporous Mater. 232 (2016) 13–25, https://doi.org/10.1016/j.micromeso.2016.06.002.
[42] T.M. Díez-Rodríguez, E. Blázquez-Blázquez, R. Barranco-García, E. Pérez, M. L. Cerrada, Macromol. Mater. Eng. (2022) 2200308, https://doi.org/10.1002/mame.202200308.
[43] S. Rathi, J.P. Kalish, E.B. Coughlin, S.L. Hsu, Macromolecules 44 (2011) 3410–3415, https://doi.org/10.1021/ma2003135.
[44] J.D. Badia, L. Santonja-Blasco, A. Martínez-Felipe, A. Ribes-Greus, Polym. Degrad. Stabil. 97 (2012) 1881–1890, https://doi.org/10.1016/j.polymdegradstab.2012.06.001.
[45] T.M. Díez-Rodríguez, E. Blázquez-Blázquez, J.C. Martínez, E. Pérez, M.L. Cerrada, Polymer 241 (2022) 124515, https://doi.org/10.1016/j.polymer.2022.124515.
[46] F.J.B. Calleja, Adv. Polym. Sci. 66 (1985) 117–148, https://doi.org/10.1007/3-540-13779-3_19.
[47] C. Fonseca, J.M. Pereña, R. Benavente, M.L. Cerrada, A. Bello, E. Pérez, Polymer 36 (1995) 1887–1892, https://doi.org/10.1016/0032-3861(95)90936-V.
[48] G. Li, Y. Guo, X. Sun, T. Wang, J. Zhou, J. He, J. Phys. Chem. Solid. 73 (2012) 1268–1273, https://doi.org/10.1016/j.jpcs.2012.06.013.
[49] Y. Tian, J. Qi, W. Zhang, Q. Cai, X. Jiang, ACS Appl. Mater. Interfaces 6 (2014) 12038–12045, https://doi.org/10.1021/am5026424.
[50] W. Guo, X. Li, X.S. Zhao, Microporous Mesoporous Mater. 93 (2006) 285–293, https://doi.org/10.1016/j.micromeso.2006.03.009.
[51] D. Margolese, J.A. Melero, S.C. Christiansen, B.F. Chmelka, G.D. Stucky, Chem. Mater. 12 (2000) 2448–2459, https://doi.org/10.1021/cm0010304.
[52] Q. Yang, J. Liu, J. Yang, L. Zhang, Z. Feng, J. Zhang, C. Li, Microporous Mesoporous Mater. 77 (2005) 257–264, https://doi.org/10.1016/j.micromeso.2004.09.009.
[53] V.D. Hoang, T.P. Dang, Q.K. Dinh, H.P. Nguyen, A.T. Vu, Adv. Nat. Sci. Nanosci. Nanotechnol. 1 (2010) 035011, https://doi.org/10.1088/2043-6262/1/3/035011.
[54] L. Chaabane, M. Nikolantonaki, G. Weber, I. Bezverkhyy, R. Chassagnon, A. Assifaoui, F. Bouyer, J. Taiwan Inst. Chem. Eng. 152 (2023) 105169, https://doi.org/10.1016/j.jtice.2023.105169.
[55] A.J. Ryan, J.L. Stanford, W. Bras, T.M.W. Nye, Polymer 38 (1997) 759–768, https://doi.org/10.1016/j.polymer.2022.125232.
[56] T.M. Díez-Rodríguez, E. Blázquez-Blázquez, J.C. Martínez, M.L. Cerrada, E. Pérez, Polymer 256 (2022) 125232, https://doi.org/10.1016/j.polymer.2022.125232.
[57] P. Pan, B. Zhu, W. Kai, T. Dong, Y. Inoue, Macromolecules 41 (2008) 4296–4304, https://doi.org/10.1021/ma800343g.